ChemistryOPEN

Supporting Information

Immobilization of Cellulase on Magnetic Nanocarriers

Hans-Christian Roth[+], Sebastian P. Schwaminger[+], Fei Peng, and Sonja Berensmeier*[a]

open_201600028_sm_miscellaneous_information.pdf

Experimental

Materials

Ferric chloride ($FeCl_3 \cdot 6\ H_2O$), sodium hydroxide (NaOH), acetic acid and di-ammonium hydrogen citrate were purchased from AppliChem GmbH, Germany. Ferrous chloride ($FeCl_2 \cdot 4H_2O$), tetraethyl orthosilicate (TEOS), sodium acetate (NaAc) and cellulase (CEL) (EC 3.2.1.4) (16 U g^{-1} at pH 5 and 37°C) were purchased from Sigma-Aldrich. P-nitrophenol (pNP) and pNP-cellobioside were purchased from ABCR. Sodium chloride (NaCl), sodium carbonate, ammonia, ethanol and hydrochloric acid (HCl) were purchased from Roth.

Synthesis

Superparamagnetic iron oxide nanoparticles (MNP) were synthesized by the co-precipitation of Fe^{2+} and Fe^{3+} aqueous salt solutions in an alkaline environment. Aqueous solutions of ferrous chloride (100 mL, 1 M), ferric chloride (100 mL, 2 M) and sodium hydroxide (500 mL, 1 M) were prepared with degassed and deionized water. The precipitation of MNP was performed in a Mettler Toledo Optimax reactor under nitrogen atmosphere to prevent oxidation of the precursors and the product.

For the preparation of silica-coated MNP (MNP@SiO), the MNP suspension (0.5 g L^{-1}) was stabilized with a 50 g L^{-1} di-ammonium hydrogen citrate buffer and adjusted to a pH of 8.8 with ammonia. Subsequently, the suspension was sonicated for 1 h with a Branson Digital Sonifier S4500D in a Mettler Toledo Optimax reactor. 1 mL TEOS was dissolved in 10 mL ethanol and added dropwise to the magnetite suspension, which was hold at 60°C and stirred with 800 rpm for 3 h.

For the enzyme immobilization, 0.5 g L^{-1} of particle suspension was mixed with CEL in a Mettler Toledo Optimax reactor in a 50 mM buffered sodium acetate solution at pH 5. The mixture was stirred for 24 h at 60°C at 800 rpm after sonication for 1 h.

Characterization

Attenuated total reflection infra-red (ATR-IR) spectroscopy spectra were recorded with a liquid nitrogen cooled Bruker Vertex 70 FTIR-spectrometer with a single reflection Platinum ATR accessory from Bruker using 64 scans in a region of 4000 cm^{-1} to 550 cm^{-1}.

X-ray photoelectron spectroscopy (XPS) analysis was conducted in UHV (below $5x10^{-8}$ mbar) in a Leybold-Heraeus LHS-10 chamber with a non-monochromatized Al Kα cathode. Powder samples were prepared on a sticky copper tape. Survey spectra were scanned five times with a step width of 1 eV while detail spectra were scanned 30 times with a step width of 0.1 eV. All measurements were conducted with a pass energy of 100 eV.

Simultaneous thermal analysis (STA) was performed with a Netzsch Jupiter 449 C apparatus at a heating rate of 10 K min^{-1} in a nitrogen flow of 30 mL min^{-1} in aluminum oxide pans. Mass signals were detected with a Netzsch Äeolos QMS 403.

Transmission electron microscopy (TEM) micrographs were generated with a JEOL 100 CX and processed with the software ImageJ. TEM samples of dispersed particles were drop-casted onto a holey carbon coated copper grid (Quantifoil) and the solvent was evaporated.

Superconducting quantum interference device (SQUID) magnetometric measurements were performed with a Quantum Design MPMS 5XL magnetometer between - 50 kOe and 50 kOe at 300 K. Therefore, samples were mounted into a straw in a gelatin capsule.

Dynamic light scattering (DLS) and zeta potential were measured with a Beckman Coulter Delsa Nano C Particle Analyzer. Samples were prepared using 0.5 g L^{-1} of the sample and diluted in water 1:10 prior to the application. Sonication was used to disperse the samples. One measurement consists of a statistic analysis of the results of three measuring cycles with 70 single measurements. Zeta potential was recorded from pH 10 to pH 3 with HCl and NaOH as titrands.

X-ray diffraction (XRD) diffractograms were measured with a STOE Stadi P diffractometer and a Mo Kα source in transmission geometry.

The specific surface area was determined with a Micromeritics Gemini VII 2390 Surface Area Analyzer. Prior to analysis, the samples were dried in a vacuum at 100°C and weighed. The measurement included a determination of the sample volume with the inert gas helium and the gas adsorption isotherm of nitrogen at 77 K. From the gas adsorption isotherms the specific surface area was determined by the Brunauer Emmet Teller (BET) method.

Potentiometric titrations were accomplished under nitrogen atmosphere in a stirred tank reactor from pH 4 to 10. Sodium hydroxide and hydrochloric acid were used as titrands and the ionic strength was adjusted to either 10 or 100 mmol L^{-1} NaCl.

The phenanthroline assay is a photometric detection of iron ions by formation of an iron-phenanthroline complex. MNP and MNP@Silica samples were dissolved in concentrated hydrochloric acid (37 %) with a subsequent reduction of iron ions to Fe^{2+} by ascorbic acid in an acetate buffer (pH 4.5). Addition of phenanthroline solution to the dissolved iron ions at pH 4.5 led to the formation of a reddish-colored iron complex. In order to determine the concentration of iron ions, absorbance was measured by a Magellan Infinite 200 photometer (Tecan Trading AG) at 510 nm.

Adsorption isotherms of CEL on both carrier materials (MNP and MNP@SiO) were conducted in a buffered sodium acetate solution (50 mM, pH 5). Therefore, 1000 µL of particle suspension (2 g L^{-1}) were incubated with 1000 µL of identically buffered CEL solution (0.05 – 8 g L^{-1}). Incubation was performed in a shaking incubator (Eppendorf Thermomixer) at 1000 rpm and 50°C for 10 h. Resulting CEL-particle composites are referred as nano-biocatalysts (NBC) and differentiated according to the carrier materials as NBC_{MNP} and NBC_{SiO}.

For the *p*-nitrophenol (*p*NP) assay, 1000 µL of buffered CEL solution (0.1 g L^{-1} – 4 g L^{-1}) and NBC suspensions (1 g L^{-1}) were preheated for 1 min at 50°C and incubated with 200 µL of pNP-cellobioside (2 mmol L^{-1}) for 10 min at 50°C and 1000 rpm in a shaking incubator. The enzymatic reaction was terminated by cooling the samples in ice for 1 min. Subsequently, CEL solutions were centrifuged at 10000 G while the NBCs were separated magnetically from the supernatant. After the addition of 100 µL sample supernatant to 100 µL Na_2CO_3 solution (1 M), the amount of enzymatically released *p*NP was detected by an Infinite M200 Photometer at 405 nm.

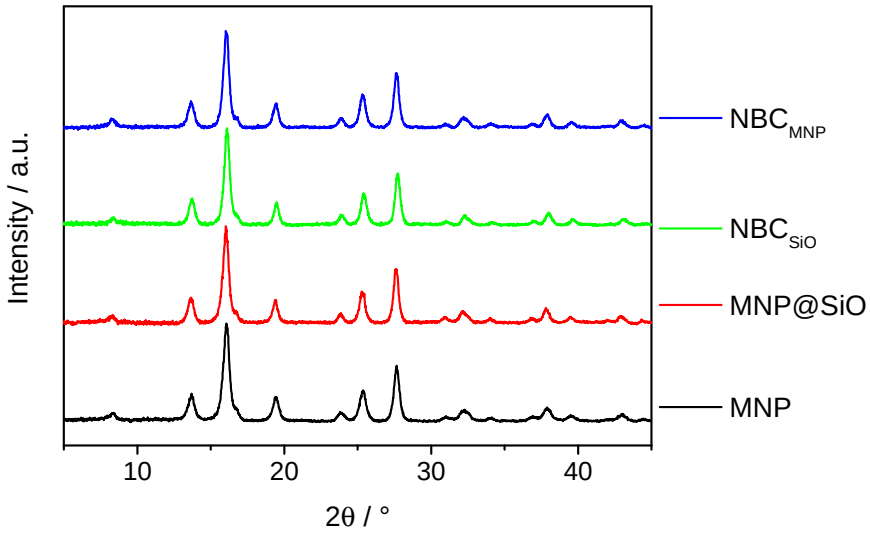

Figure S1. Transmission X-ray diffractograms of dried MNP, MNP@SiO, NBC_{MNP} and NBC_{SiO} conducted with a MoKα-source.

X-ray diffractograms demonstrate the same reflexes for all materials investigated, indicating no alteration of primary particles over all coating and immobilization processes. While the reflexes evidence the existence of the inverse spinel magnetite (JCPDS card no. 85-1436) (220 / 3°, 311 / 16°, 400 / 19°) no hematite can be observed and also no sign of a mild oxidation to maghemite is demonstrated in the diffractogram. Furthermore, the primary particle diameter, which can be calculated from the Scherrer equation (11 nm), matches for all four samples. No reflexes can be assigned to the amorphous silica coating.[1]

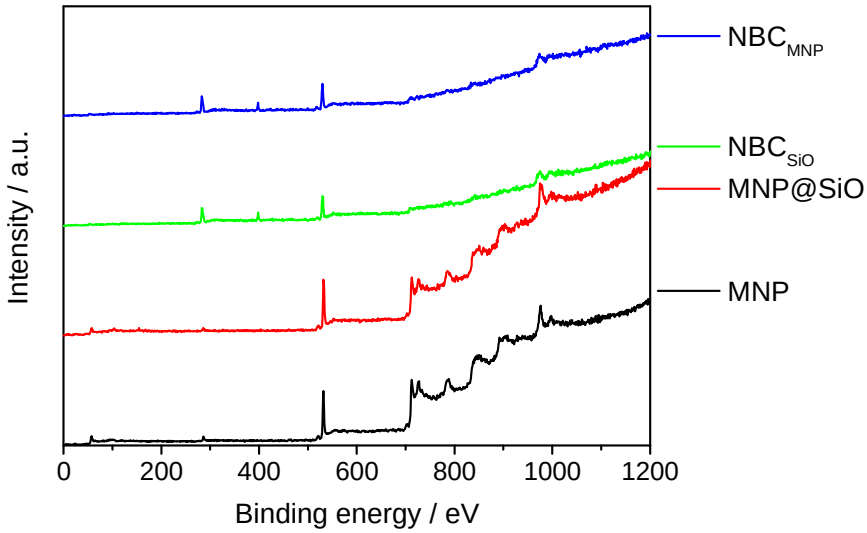

Figure S2. XP survey spectra of dried MNP, MNP@SiO, NBC$_{MNP}$ and NBC$_{SiO}$ with an AlKα-source in UHV. Each spectrum is measured 5 times with 1 eV steps and a pass energy of 100 eV.

Survey spectra indicate iron oxide species for all samples while strong peaks are visible for MNP and MNP@SiO. For the MNP@SiO particles a small peak corresponding to silicon can be observed around 104 eV .The carbon peak (285 eV) increases for both NBCs compared to bare nanoparticles and moreover a nitrogen peak (400 eV) appears.

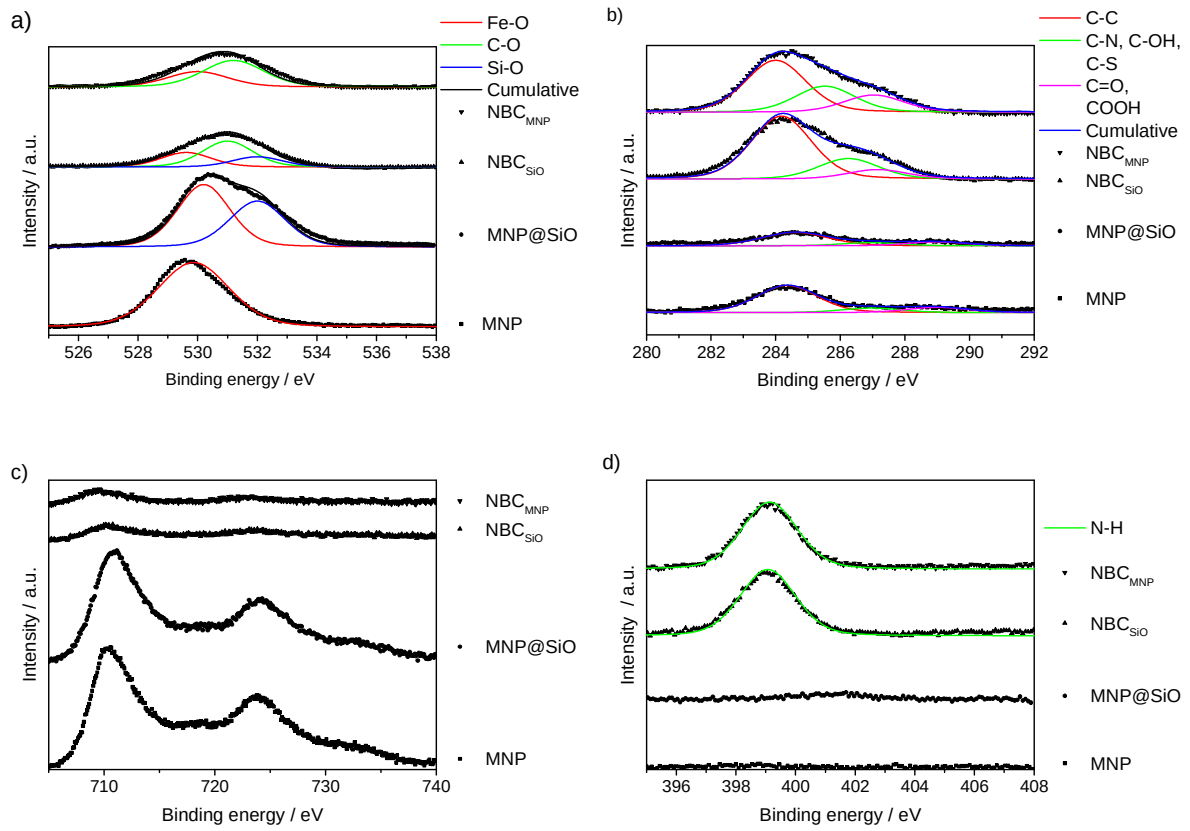

Figure S3. XP spectra in the **a)** O 1s region **b)** C 1s region **c)** Fe 2p region **d)** N 1s region of dried MNP, MNP@SiO, NBC_{MNP} and NBC_{SiO} with an AlKα-source in UHV.

The O 1s spectra reveal different oxygen species due to chemical shifts. Beside the Fe-O species (530 eV) which is evident for all samples, carbon bound oxygen (531 eV) is visible for NBCs. Si-O species (532 eV) can only be observed for the silica coated particles and the peak intensity is an indicator for a homogeneous coating. The C 1s spectra indicate the cellulase immobilization on the NBC species as the carbon peak increases while only adventitious carbon species (284.5 eV) can be observed on the bare nanoparticles. Furthermore, chemically shifted carbon species such as C-N, C-S and C-OH (286 eV) and carboxyl/amide groups (288 eV) can be observed for the NBC samples.[2] All Fe 2p spectra demonstrate Fe-O shifts (712 eV and 724 eV) which do not change significantly with coating and immobilization.[3] Especially the low satellite peak at 717 eV evidences the presence of magnetite and therefore excludes hematite as Fe-O species.[3] From these spectra, a distinction between magnetite and maghemite is not possible. Nitrogen peaks (399.5 eV) are only visible for NBCs which evidences the presence of enzyme in these samples.[4]

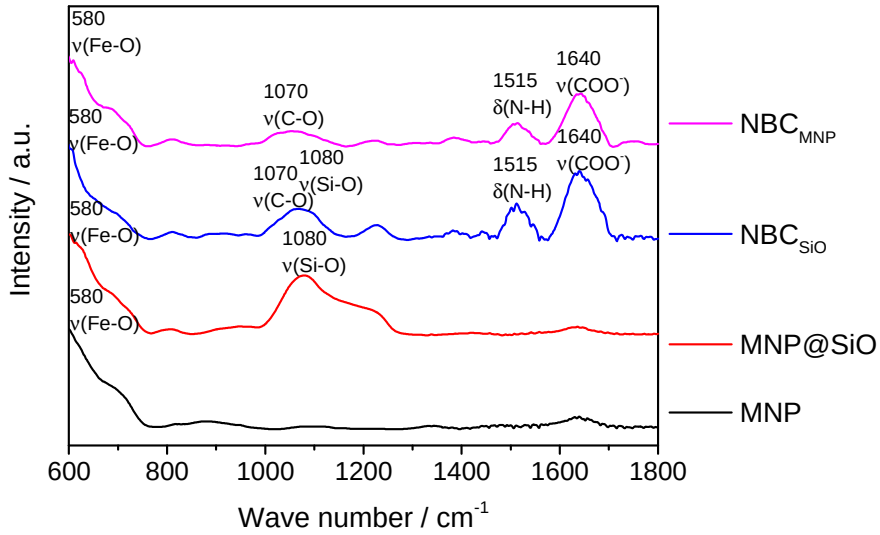

Figure S4. ATR-IR spectra of MNP, MNP@SiO, NBC_{SiO} and NBC_{MNP} measured on a single reflex diamond ATR unit.

ATR-IR spectroscopy facilitates a good possibility to follow the coating and immobilization steps. For the MNPs only bands corresponding to Fe-O vibrations (T_{1u}) are visible.[5] The silica coating can be verified by a strong band at 1080 cm^{-1} corresponding to a Si-O-Si stretching vibration.[6] Furthermore, the immobilization is illustrated by amide bands (1515 and 1630 cm^{-1}) and C-O bands corresponding to glycosylations of proteins at 1070 cm^{-1}.[1,7]

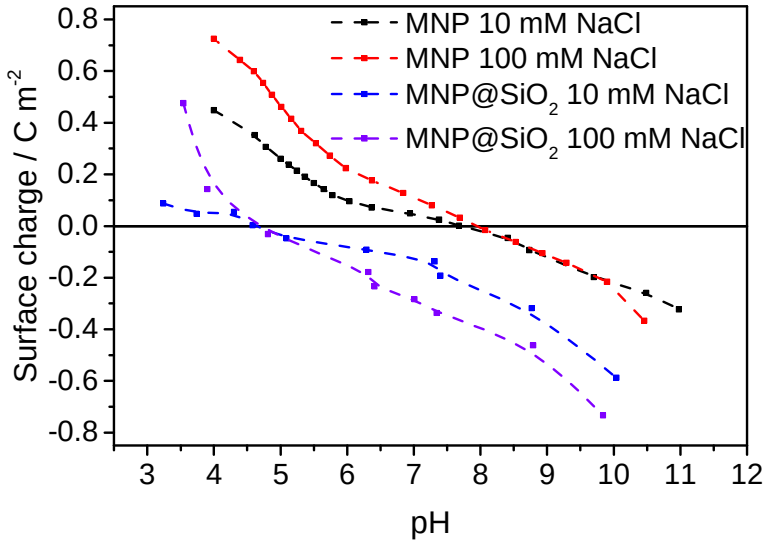

Figure S5. Potentiometric acid-base titrations of MNP and MNP@SiO at different NaCl amounts with the titrands HCl and NaOH.

The point of zero charge of bare magnetite nanoparticles shifts from pH 7.8 to 4.6 with the silica coating which is ensued by potentiometric titrations at different ionic strengths.

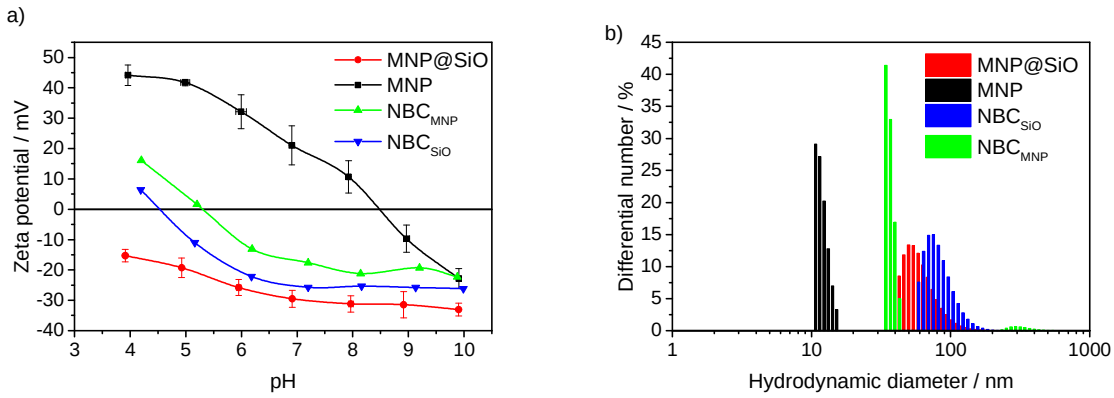

Figure S6. a) zeta potential and **b)** DLS measurements of MNP, MNP@SiO, NBC_{SiO} and NBC_{MNP} in sodium acetate buffer. Error bars derive from zeta potential measurements conducted in triplicate (±SD).

The isoelectric point (IEP) for bare MNPs ranges between pH 8 and 9 which is in good agreement with literature.[8] The coating of nanoparticles with silica leads to a negatively charged surface in the pH range 3 to 10.[9] The adsorption of cellulase leads to an IEP around pH 5[10] and an almost similar behavior of NBC_{MNP} and NBC_{SiO} over

the pH range 3-10. The slight difference between the zeta potential of different NBC species can be explained by the interaction of different protein side chains with the particle surfaces and therefore differently charged terminal side chains. The hydrodynamic diameter for the number distribution of bare nanoparticles is in the range of 12-15 nm. The silica coating enlarges the primary particle diameter, and so agglomeration effects occur for MNP@SiO at pH 5 as the surface is less charged than bare MNPs. Hence, the particle distribution broadens for the coated particles around 50 nm. The adsorption of cellulase shifts the hydrodynamic particle diameter to around 35 nm and 70 nm for NBC_{MNP} and NBC_{SiO} respectively.

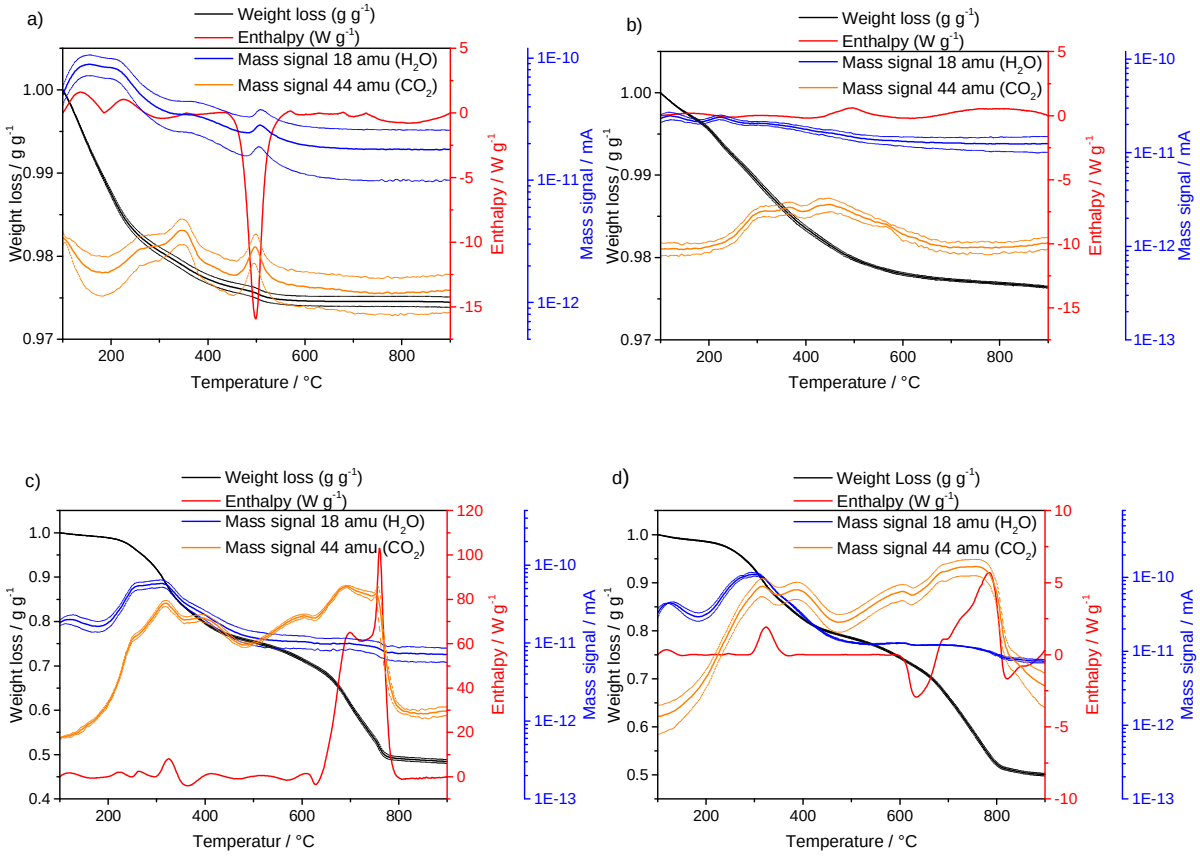

Figure S7. STA-MS data of **a)** MNP **b)** MNP@SiO **c)** NBC_{SiO} **d)** NBC_{MNP}. Overlay of TG, DSC signal and mass traces 18 and 44 amu corresponding to H_2O and CO_2. Error bars derive from STA measurements conducted in triplicate (±SD).

The freeze-dried MNP demonstrate a weight loss of ca. 2%, which can be related to bound water on the surface.[1] The water is evidenced by the mass signal 18 (m/z) which increases by around 200°C and is accompanied by the biggest weight loss and

an exothermic DSC signal. The strong endothermic DSC signal around 500°C can be assigned to a phase transition of magnetite[11] and a hydrolytic reaction is possible as the mass signal at 18 amu increases. Furthermore, two peaks corresponding to CO_2 (44 amu) can be detected around 300 and 400°C due to adventitious carbon. MNP@SiO show less adventitious carbon compared to the bare MNP as in addition indicated by XPS. Furthermore, a lesser water content could be verified on these samples and no DSC signal appears during the heating at 500°C. Therefore we assume an entire coating of the MNP by silica. The adsorbed cellulase in NBC_{SiO} demonstrates two protein decay and desorption regions which can be detected by an increase in the mass signal corresponding to CO_2. Furthermore, desorption and decomposition of protein is emphasized by endothermic DSC signals at 300, 700 and 750°C.[1] Interestingly, the enthalpy of NBC_{SiO} at 700 and 750°C is much higher than the enthalpy of NBC_{MNP} indicating a different and stronger bonding between surface and cellulase. The weight loss in both NBC species is similar but with around 50 % higher than the adsorption indicated by the photometric detection of supernatants. This behavior can be explained by the bound water within the protein and between cellulase and particle surface and is linked to a higher MS signal for water.

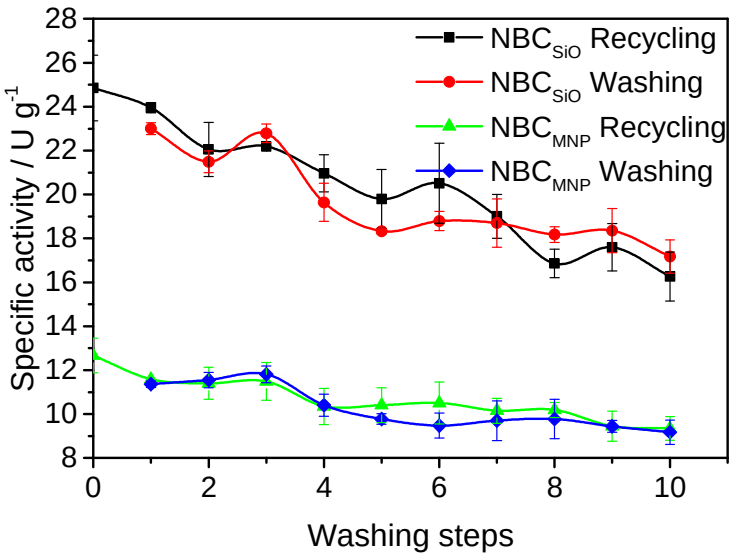

Figure S8. Specific activity of NBC over 10 cycles. Comparison between reuse of NBC and washing effect. Error bars derive from *p*NP assays conducted in triplicate and the photometric analysis of three samples for each assay (±SD).

The specific activity of NBCs was checked after each recycling step and was additionally compared to NBCs that were merely washed as often as the recycled particles but never reused. The specific activity of NBC_{SiO} decreases from 25 to 16 U g^{-1} while the specific activity of NBC_{MNP} decreases from 13 to 9 U g^{-1}. These effects can be related to the total NBC loss that occurs for each washing step and the enzymes do not lose activity due to inactivation or decomposition. The supernatant was therefore checked with a photometer after each washing step and no protein was detected.

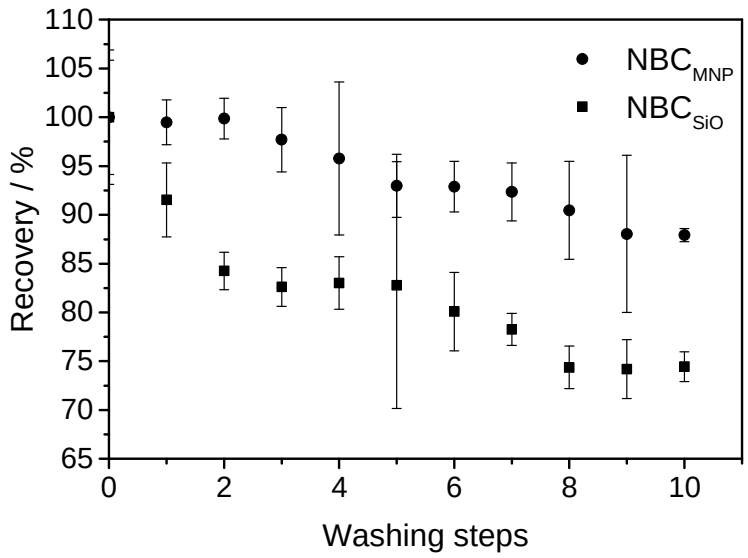

Figure S9. Recovery efficiency of NBC determined by a phenanthroline assay. Error bars derive from phenanthroline assays conducted in triplicate and the photometric analysis of three samples for each assay (±SD).

The iron content of NBCs was checked after each washing step with a phenanthroline assay. The recovery efficiency for NBC_{SiO} was lower than NBC_{MNP} which can be explained by a lower saturation magnetization of the silica-coated particles. However, a recovery of 75 % for NBC_{SiO} after 10 double washing steps is still higher than most comparable NBC systems in the literature.[12]

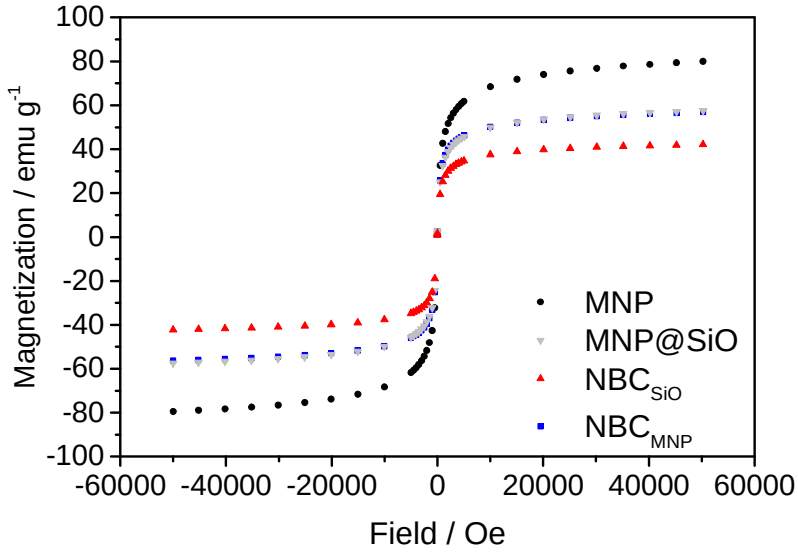

Figure S10. SQUID-magnetometry of MNP, MNP@SiO, NBC_{SiO} and NBC_{MNP} in a range from -50000 to 50000 Oe at 300 K.

SQUID data evidences superparamagnetic behavior of all particles as no hysteresis can be observed. MNP demonstrate a high saturation magnetization around 80 emu g^{-1} which is in good agreement with magnetite nanoparticles.[8,13] The silica coating reduces the magnetization to 58 emu g^{-1}. Furthermore, the adsorption of cellulase leads to a decrease in the saturation magnetization of the corresponding NBCs. NBC_{MNP} demonstrates a saturation magnetization of 57 emu g^{-1} while NBC_{SiO} shows a saturation magnetization around 42 emu g^{-1}. Both decreases in magnetization agree with the load of cellulase on the particles.

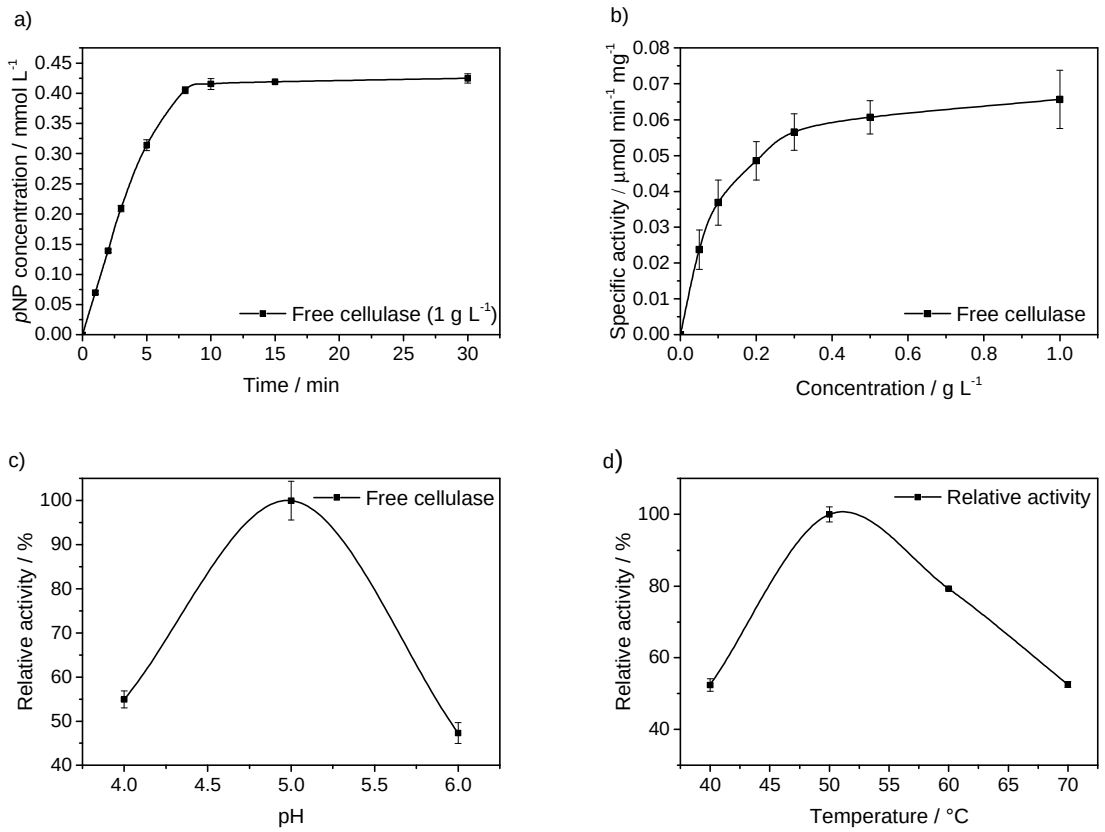

Figure S11. Determination of **a)** free cellulase activity and dependency of activity of free cellulase on **b)** concentration, **c)** pH and **d)** temperature. Error bars derive from *p*NP assays conducted in triplicate and the photometric analysis of three samples for each assay (±SD).

The cellulase kinetics for the degradation of *p*NP-cellobioside were measured over 30 minutes for 1 g L^{-1} free cellulase at pH 5 and 50°C. The slope in first three minutes results in an activity of 66 U g^{-1}. Remarkably, the concentration of cellulase plays a major role for the activity which is ascribed to channeling effects of the enzyme in the literature. These synergism effects as observed for free cellulase might be an explanation for the lower activity of NBCs.[14] We verified the optimal conditions for cellulase activity from literature being 50°C and pH 5 which decreases for different conditions.

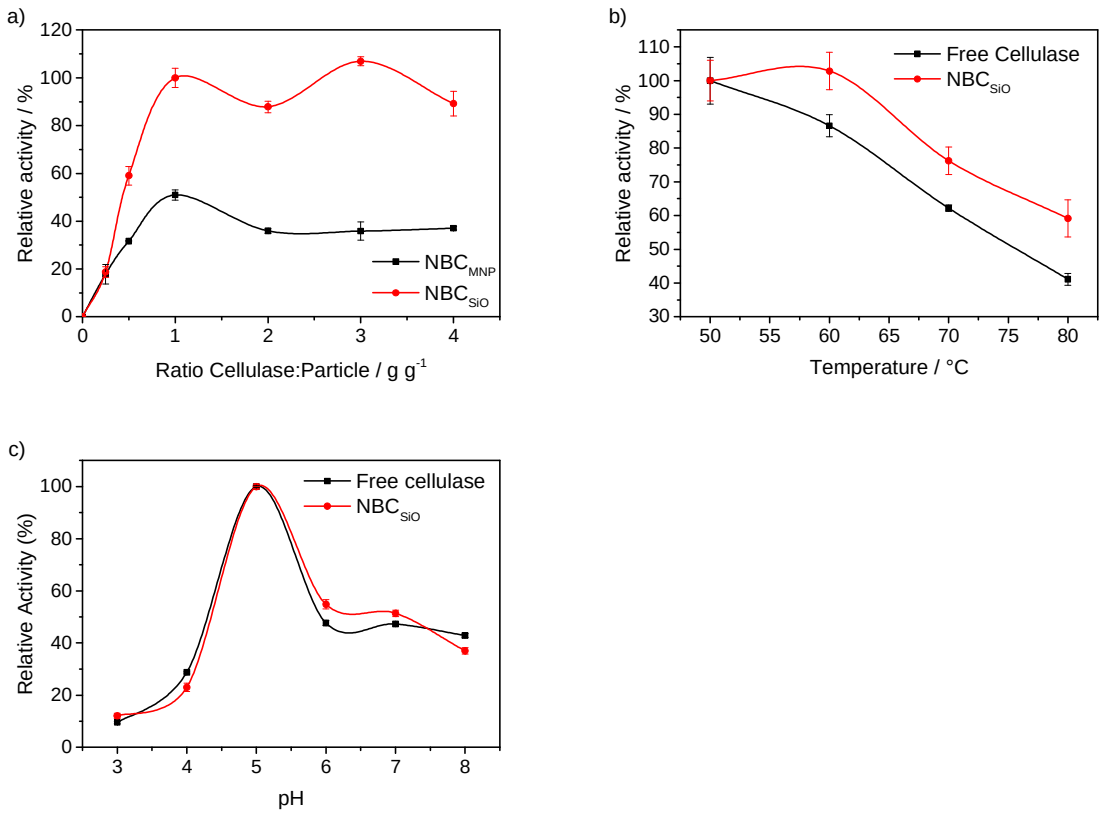

Figure S12. Dependency of the relative activity of NBCs on **a)** the immobilization ratio (cellulase : particle) and on the storage **b)** temperature and **c)** pH before the implementation of the pNP assay. Error bars derive from *p*NP assays conducted in triplicate and the photometric analysis of three samples for each assay (±SD).

The ratio of cellulase to particle influences the activity of NBCs. While the relative activity of cellulase (related to cellulase concentration) in the saturation region remains the same, the activity is lower for lower cellulase loads. The behavior for NBC_{MNP} and NBC_{SiO} for different cellulase to particle ratios are approximately similar and is in good agreement with the influence of the concentration on the free cellulase. The storage at different pH value for 1 hour before use resulted in lower activities for bound and unbound cellulase in the same dimensions. On the other hand, NBC_{SiO} demonstrated a better temperature stability than free cellulase which is known in the literature for comparable NBC systems.[13]

[1] P. Esmaeilnejad-Ahranjani, M. Kazemeini, G. Singh, A. Arpanaei, *RSC Adv.* **2015**, *5*, 33313–33327.
[2] R. Turcu, V. Socoliuc, I. Craciunescu, A. Petran, A. Paulus, M. Franzreb, E. Vasile, L. Vekas, *Soft matter* **2015**, *11*, 1008–1018.

[3] A. P. Grosvenor, B. A. Kobe, M. C. Biesinger, N. S. McIntyre, *Surf. Interface Anal.* **2004**, *36*, 1564–1574.
[4] Y. Ren, J. G. Rivera, L. He, H. Kulkarni, D.-K. Lee, P. B. Messersmith, *BMC Biotechnol.* **2011**, *11*, 63.
[5] A. M. Jubb, H. C. Allen, *ACS Appl. Mater. Interfaces* **2010**, *2*, 2804–2812.
[6] P. Innocenzi, *J. Non-Cryst. Solids* **2003**, *316*, 309–319.
[7] a) M. Khajehpour, J. L. Dashnau, J. M. Vanderkooi, *Anal. Biochem.* **2006**, *348*, 40–48; b) V. Zlateski, R. Fuhrer, F. M. Koehler, S. Wharry, M. Zeltner, W. J. Stark, T. S. Moody, R. N. Grass, *Bioconjugate Chem.* **2014**, *25*, 677–684.
[8] R. M. Cornell, U. Schwertmann, *The iron oxides*. *Structure, properties, reactions, occurrences, and uses*, Wiley-VCH, Weinheim, **2003**.
[9] F. S. Emami, V. Puddu, R. J. Berry, V. Varshney, S. V. Patwardhan, C. C. Perry, H. Heinz, *Chem. Mater.* **2014**, *26*, 5725–5734.
[10] O. Kudina, A. Zakharchenko, O. Trotsenko, A. Tokarev, L. Ionov, G. Stoychev, N. Puretskiy, S. W. Pryor, A. Voronov, S. Minko, *Angew. Chem. Int. Ed.* **2014**, *53*, 483–487*; Angew. Chem.* **2014***, 126*, 493–497.
[11] J. B. Mamani, A. J. Costa-Filho, D. R. Cornejo, E. D. Vieira, L. F. Gamarra, *Mater. Charact.* **2013**, *81*, 28–36.
[12] J. Jordan, C. S. Kumar, C. Theegala, *J. Mol. Catal. B: Enzym.* **2011**, *68*, 139–146.
[13] H.-C. Roth, S. P. Schwaminger, M. Schindler, F. E. Wagner, S. Berensmeier, *J. Magn. Magn. Mater.* **2015**, *377*, 81–89.
[14] U. Bornscheuer, K. Buchholz, J. Seibel, *Angew. Chem. Int. Ed.* **2014**, *53*, 10876–10893*; Angew. Chem.* **2014***, 126*, 11054–11073.